Published in final edited form as:
Conf Proc IEEE Int Conf Syst Man Cybern. 2013 ; : 1488–1493. doi:10.1109/SMC.2013.257.

Automatic Steering of Manually Inserted Needles

Guofan Wu,
Dept. of Mechanical Engineering, Carnegie Mellon University, Pittsburgh, PA 15213 USA

Xiao Li,
Dept. of Mechanical Engineering, Carnegie Mellon University, Pittsburgh, PA 15213 USA

Craig A. Lehocky, and
Dept. of Biomedical Engineering, Carnegie Mellon University, Pittsburgh, PA 15213 USA

Cameron N. Riviere
The Robotics Institute, Carnegie Mellon University, Pittsburgh, PA 15213 USA

Guofan Wu: gwu@andrew.cmu.edu; Xiao Li: xl1@andrew.cmu.edu; Craig A. Lehocky: calehocky@cmu.edu; Cameron N. Riviere: camr@ri.cmu.edu

Abstract

Bevel-tipped flexible needles can be robotically steered to reach clinical targets along curvilinear paths in 3D. Manual needle insertion allows the clinician to control the insertion speed, ensuring patient safety. This paper presents a control law for automatic 3D steering of manually inserted flexible needles, enabling path-following control. A look-ahead proportional controller for position and orientation is presented. The look-ahead distance is a linear function of insertion speed. Simulations in a 3D brain-like environment demonstrate the performance of the proposed controller. Experimental results also show the feasibility of this technique in 2D and 3D environments.

Keywords

medical robotics; controls; path tracking; needle steering

I. Introduction

Many important diagnoses and treatments are accomplished by needle insertion [1]. In the brain, needle insertion is important as a possible delivery technique for chemotherapy [2]. Straight, quasi-rigid needles have traditionally been used for many applications. If the needles used were flexible and could be steered, the resulting ability to follow curved trajectories would enable the needle to avoid critical anatomical structures, greatly increasing the set of feasible trajectories. Flexible needles with beveled tips, as is common, curve during insertion due to the asymmetry of the tip. Webster et al. exploited in order to steer needles by dynamically reorienting the needle shaft [3]. Our group augmented this technique, adding proportional control of curvature by rotating needles with a duty cycle during insertion [4], [5].

Among other possibilities, a steerable needle could be used as a guide wire for deep brain stimulation (DBS) [6]. In some DBS cases, surgeons start near Kocher's point (2.5 cm off

the midline at the level of the coronal suture) and aim for the subthalamic nucleus. The nearby corticospinal tract must be avoided. Such a DBS scenario is used in this paper to establish the geometry for planning and experiment. Figure 2 illustrates the environment, consisting of a simplified set of anatomical obstacles: the basal ganglia, corticospinal tracts, and the thalamus [7].

Needle trajectories in clinical use will generally be planned preoperatively. Numerous algorithms have been developed to plan trajectories for steerable needles [8–13]. Once a feasible path is determined, closed-loop path-following control is needed in order to execute the desired trajectory safely and effectively. Of the relevant literature on path planning, some papers do not address control explicitly; some others include it; some others accomplish control indirectly by rapid replanning. The techniques in these papers have been developed generally for insertion at constant speed, which is most compatible with motorized insertion. Surgeons may prefer to insert needles manually, in order to preserve force feedback or for other reasons related to safety [14], [15]. In this paper, we present a control technique suitable for automatic steering control of manually inserted needles, providing appropriate path-following in the presence of time-varying insertion speed.

Okazawa *et al.* developed a handheld needle steering device which was an early example of a simple concentric tube robot [16]; the presentation did not deal with path-following control. The earliest demonstrations of needle steering via duty-cycled rotation were done with manual insertion, but these involved open-loop execution of trajectories at various curvatures, with no path-following control [4], [17]. Kallem and Cowan parameterized a needle steering control algorithm in terms of insertion distance rather than time, in order to make the system easily compatible with manual insertion [18]. However, this work did not deal with proportional control of steering radius using duty-cycled rotation. Incorporation of duty-cycled rotation in the control system during manual insertion creates significant additional difficulties in handling transitions between duty cycle periods and control of rotational speed under variation in insertion speed; this paper presents a practical control system that specifically addresses these challenges.

II. Methods

The hardware system is shown in Figure 1. The clinician controls the insertion of the needle by pushing the handgrip forward. The system has a single motor, which is used for axial rotation of the needle; this motor performs the duty-cycled rotation and also reorientation of the needle as needed in order to control the direction of bending. (A second motor for insertion can be added when needed, in order to perform tests with motorized insertion, for comparison, as in Section V.) A telescopic sheath is used to prevent buckling of the flexible needle outside the tissue. An orthogonally mounted stereo pair of cameras and a PC user interface provide the surgeon real-time visual feedback about estimated states and path-tracking errors.

III. 3D Kinematic Model of Bevel-tipped Needle

The nonholonomic kinematics of the insertion of flexible bevel-tipped needles has been described by Webster *et al* [3]. As presented in Fig. 3, a body coordinate frame Ω is rigidly

attached to the needle tip. The body *x*-axis is the direction of insertion, the *y*-axis is the bending direction, and the *z*-axis is determined by the right-hand rule. Inserting the needle causes the tip to move along the *x*-axis with velocity *v* and rotate about the *z*-axis with angular velocity *v*/*r*, where *r* is the radius of curvature for the needle in that particular tissue. The maximum possible curvature is $\kappa_{max}=1/r_{min}$; r_{min} is the minimum attainable radius, which corresponds to insertion without axial rotation ($\omega = 0$). Through duty-cycled rotation, the needle can achieve any curvature between 0 and κ_{max}.

In this work, the insertion velocity is not constant and manipulated by the human operator. In real clinical situations, a typical range of insertion velocity is between 0.2 and 1.8 mm/s [19]. The effect of velocity variation on the needle curvature has been shown to be negligible [20].

IV. Control System Design

Based on the kinematic model [3], we design a control system for the manual insertion as depicted in Fig. 4.

The main difference between the previous needle steering system [5], [21] and this prototype for manual insertion lies in the loss of one control input: the insertion distance. To compensate for this drawback, an added sensor (Temposonics® EP2 magnetostrictive linear position sensor) is used to provide additional information.

The control flow (Fig. 4) is as follows: a feasible trajectory from the entry zone to the clinical target is generated using RRT, which provides the desired position and orientation of each point on the path. Stereo cameras and the magnetic displacement sensor keep track of the tip position and insertion length. Based on the sensor data, state estimation is performed using an extended Kalman filter (EKF) and a low-pass differentiator. By comparing the estimated state with the reference point on the preplanned path, the cross-track error and heading error are calculated for the controller to determine the appropriate rotational duty cycle and final orientation angle for each duty-cycling period in order to follow the path. More detailed descriptions are given in the following sections.

A. Error Calculation for Manual Insertion

For manual insertion control, the path planner is separated from the control block. The key issue for error calculation is the selection of a reference point on the planned trajectory for comparison. In our previous work, the nearest point to the tip is selected. This work uses a modified version of the error calculation. As Fig. 5 indicates, a look-ahead distance is added. The steps in the error calculation are as follows:

- **a.** Find the nearest point (blue point in Fig. 5) on the planned path to the current tip position.
- **b.** Calculate a look-ahead distance, *L*, which is related to the current insertion velocity by a model with saturation

$$L = \min\{kv, L_{\max}\}$$

where $L_{\max}$ represents a threshold.

c. Search forward on the planned path to find the point (the green one in Figure 5) that is at a distance L forward of the closest point on the path.

The look-ahead distance is introduced to compensate for time delay. By comparing the reference point with the current tip, we can calculate the same errors defined in [21]: position error (or "cross-track" error [22]) and heading error.

The position error, e_{rf}, is the distance from the tip frame to the reference frame in the given trajectory. The heading error, φ_e, is the angle between the x-axis at the needle tip and the tangent to the planned path at the reference point. Since both position error and heading error can be reduced through rotation of the needle (duty-cycled rotation and/or reorientation), a weighting scheme for rotation angle and desired curvature is used [21]. For simplicity, we represent the position and orientation of the reference as (e_{xrf}, e_{yrf}, e_{zrf}) and (q_{0rf}, q_{xrf}, q_{yrf}, q_{zrf}) in the tip frame, where quaternion representation is used. These two vectors reflect the two aspects of tracking error: the former indicates the current "tracking" performance of tip position with the preplanned path, while the latter one tells how to adjust the heading for the next step. These two factors are combined in the controller system as shown below.

a) Position Tracking Controller—

$$\kappa_p = K_p \frac{e_{rf}}{ds}$$
$$\theta_p = \arctan(e_{zrf}, e_{yrf})$$

where K_p is the tracking gain, ds the distance moved per cycle, and e_{rf} the relative distance.

b) Heading Controller—

$$\kappa_h = K_h \tan(\varphi_e)$$
$$\theta_h = \arctan(-q_{yrf}, q_{zrf})$$

where K_h is the heading gain and φ_e the angle between the x-axis at the needle tip and the tangent to the planned path at the reference point as mentioned before.

c) Overall Controller—

$$X = \kappa_p \cos(\theta_p) + \kappa_h \cos(\theta_h)$$
$$Y = \kappa_p \sin(\theta_p) + \kappa_h \sin(\theta_h)$$
$$\theta_{total} = \arctan(Y, X)$$
$$\kappa_{total} = \max\{\sqrt{X^2 + Y^2}, \kappa_{\max}\}$$

where θ_{total} and κ_{total} serve as the inputs for motor control.

B. Motor Control

With the parameters in the previous section, this motor controller provides two outputs: the angle to rotate and the amount of curvature. Since the rotation motor is the only actuator in this system, its control algorithm must be robust enough to handle different situations. The control inputs of the motor are rotation angle and duration of rotation, so the controller outputs must be converted into these parameters.

Because the manual insertion speed is time-varying and somewhat unpredictable, when performing the duty-cycled rotation, execution time is of the essence. In the previous two-motor system, reorientation of the needle to adjust the steering direction was performed separately from duty-cycled rotation. In the present work, the adjustment of tip orientation and the duty-cycled rotation are merged into a single rotation, as depicted in Fig. 6.

In practice, we set the orientation angle and the duration of rotation at discrete intervals, once per duty-cycling period. The following equations for rotation angle and duration are used.

Rotation Angle—

$$Angle: \varphi_{total} = \theta_{total} + 2\pi \cdot k$$

where k is selected such that $\varphi_{total} \in \{\varphi_{\min}, \varphi_{\max}\}$, for preset thresholds $\varphi_{\min}$ and $\varphi_{\max}$. In this way, the rotation angle is kept in an amenable range for control accuracy.

Rotation Duration—

$$DC = \begin{cases} dc_{\min} & \frac{\kappa_{total}}{\kappa_{\max}} < dc_{\min} \\ dc_{\max} & \frac{\kappa_{total}}{\kappa_{\max}} > dc_{\max} \\ \frac{\kappa_{total}}{\kappa_{\max}} & otherwise \end{cases}$$

$$Duration: \quad \tau_s = \frac{ds}{v_e}(1 - \mathrm{DC})$$

where DC represents the value of duty cycle truncated by upper and lower bounds, and v_e is the current insertion velocity.

The equations above depict additional constraints that are imposed on the values of duty cycle and rotation angle for the manually inserted case. The bounds are set in order to avoid unpredictable situations, like jerky movement within a cycle, and in order to avoid true a 100% duty cycle (continuous spinning), which would create difficulties for sensing and triggering the following cycle.

C. State Machine Representation

Figure 6 depicts motor control for one step; Figure 7 depicts the implementation of this approach for the whole insertion process, in a state-machine representation. The control loop is triggered by distance rather than time. During the process, the magnetic insertion distance

sensor samples at a high rate (100 Hz) while the motor transitions between the two states. While in the action state, the control blocks are executed.

V. Experimental Results and Discussion

A. 2D Experiments

We performed 2D experiments first, as a simplified special case of the full three-dimensional scenario. Human subjects performed insertion by pushing the handle forward. For comparison, a separate set of insertions was performed along the same planned paths, using a translation motor operating at constant speed. Four paths were planned, and the needle was inserted along the paths using both manual insertion and motorized insertion. A new gelatin sample was used for each insertion, to avoid artifacts due to previous needle tracks. Table I indicates the RMS and maximum cross-track and heading errors for the four separate trials. Fig. 8 displays the results of path tracking for all four trials in both experimental conditions.

B. 3D Simulation and Experiments

An RRT-based path planner [23] was used to plan a feasible trajectory from the entry zone to the target region in the brain for the DBS scenario.

First, simulation results showed the feasibility of the proposed 3D control scheme. In simulation, needle position measurements contained additive Gaussian noise to simulate position measurement errors (σ = 1 mm). A variable insertion velocity was also simulated with a Gaussian distribution (σ = 0.5 mm/s). The extended Kalman filter predicted needle position and heading with maximum needle curvature of 0.01 mm^{-1}. Fig. 9 is the final result of the needle following the path beginning from the entry zone of the cortex (blue circle), toward the left subthalamic nucleus, while avoiding obstacles.

Fig. 10 demonstrates the experimental results for 3D steering in a tissue simulant (gelatin). A 0.25-mm diameter solid nitinol wire, filed down to a 10° bevel, was inserted into the gelatin. The maximal curvature for this needle in this particular tissue was found to be 0.0074 mm^{-1}. The needle was inserted along two preplanned paths from the RRT in the brain simulation environment, under two separate experimental conditions (manual and motorized insertion). Table II indicates the cross-track error for both cases, as well as the final targeting error of the needle tip position to the desired location. Manual insertion results in increased error due to difficulty in responding to the time-varying and unpredictable insertion speed.

VI. Discussion

Due to considerations of safety and expense, there is a trend in robot-assisted surgery toward keeping the human in the control loop [24]. In this work, we have designed a new control approach that allows automatic 3D steering of manually inserted flexible bevel-tipped needles. The 2D experimental and 3D simulation results show the feasibility of the proposed proportional look-ahead controller. This system maximizes the ease of retraction of the needle for safety, should it be necessary. Improvements in performance will be sought by

refining the vision-based state estimator, and by incorporating a feedforward model of torsional windup [25].

Acknowledgments

Funded in part by U.S. National Institutes of Health (grant no. R21EB012209).

References

1. Abolhassani N, Patel R, Moallem M. Needle insertion into soft tissue: a survey. Med Eng Phys. 2007; 29(4):413–431. [PubMed: 16938481]
2. National Institute of Neurological Disorders and Stroke (NINDS) and National Cancer Institute. Report of the Brain Tumor Progress Review Group. 2000.
3. Webster RJ III, Kim SJ, Cowan NJ, Chirikjian GS, Okamura AM. Nonholonomic modeling of needle steering. Int J Robot Res. 2006; 25(5–6):509–525.
4. Engh JA, Podnar G, Kondziolka D, Riviere CN. Toward effective needle steering in brain tissue. Proc Annu Int Conf IEEE Eng Med Biol Soc. 2006:559–562.
5. Engh JA, Minhas DS, Kondziolka D, Riviere CN. Percutaneous intracerebral navigation by duty-cycled spinning of flexible bevel-tipped needles. Neurosurgery. Oct; 2010 67(4):1117–22. discussion 1122–3. [PubMed: 20881576]
6. Frasson L, Ko SY, Turner A, Parittotokkaporn T, Vincent JF, Rodriguez y Baena F. STING: a soft-tissue intervention and neurosurgical guide to access deep brain lesions through curved trajectories. Proc Inst Mech Eng H. 2010; 224(6):775–88. [PubMed: 20608494]
7. Lindsley, TA. Virtual Brain Model software. Albany Medical College; 2009.
8. Alterovitz R, Goldberg K, Okamura A. Planning for steerable bevel-tip needle insertion through 2D soft tissue with obstacles. Proc IEEE Int Conf Robot Autom. 2005:1652–1657.
9. Alterovitz R, Goldberg KY, Pouliot J, Hsu ICJ. Sensorless motion planning for medical needle insertion in deformable tissues. IEEE Trans Inform Technol Biomed. Mar; 2009 13(2):217–25.
10. Park W, Kim JS, Zhou Y, Cowan NJ, Okamura AM, Chirikjian GS. Diffusion-based motion planning for a nonholonomic flexible needle model. Proc IEEE Int Conf Robot Autom. 2005:4611–4616.
11. Duindam V, Xu J, Alterovitz R, Sastry S, Goldberg K. Three-dimensional motion planning algorithms for steerable needles using inverse kinematics. Int J Robot Res. 2010; 29(June):789–800.
12. Patil, S.; Alterovitz, R. Interactive Motion Planning for Steerable Needles in 3D Environments with Obstacles. Proceedings of the IEEE International Conference on Biomedical Robotics and Biomechatronics; Jan. 2010; p. 893-899.
13. Bernardes MC, Adorno BV, Poignet P, Zemiti N, Borges GA. Adaptive path planning for steerable needles using duty-cycling. Proc IEEE/RSJ Int Conf Intell Robot Syst. 2011:2545–2550.
14. Gerovichev O, Marayong P, Okamura AM. The effect of visual and haptic feedback on manual and teleoperated needle insertion. Lect Notes Comput Sci. 2002; 2488:147–154.
15. Fischer GS, Iordachita I, Csoma C, Tokuda J, Dimaio SP, Tempany CM, Hata N, Fichtinger G. MRI-Compatible Pneumatic robot for transperineal prostate needle placement. IEEE/ASME Trans Mechatron. Jun; 2008 13(3):295–305.
16. Okazawa S, Ebrahimi R, Chuang J, Salcudean SE, Rohling R. Hand-held steerable needle device. IEEE/ASME Trans Mechatron. 2005; 10(3):285–296.
17. Engh JA, Podnar G, Khoo SY, Riviere CN. Flexible needle steering system for percutaneous access to deep zones of the brain. Proc 32nd IEEE Northeast Bioeng Conf. 2006:103–104.
18. Kallem V, Cowan NJ. Image guidance of flexible tip-steerable needles. IEEE Trans Robot. 2009; 25(1):191–196. [PubMed: 20431694]
19. Casanova F, Carney PR, Sarntinoranont M. Influence of needle insertion speed on backflow for convection-enhanced delivery. J Biomech Eng. Apr.2012 134(4):041006. [PubMed: 22667681]

20. Webster RJ III, Memisevic J, Okamura AM. Design considerations for robotic needle steering. Proc IEEE Int Conf Robot Autom. 2005:3599–3605.

21. Wood N, Shahrour K, Ost MC, Riviere CN. Needle steering system using duty-cycled rotation for percutaneous kidney access. Proc Annu Int Conf IEEE Eng Med Biol Soc. 2010:5432–5.

22. Thrun S, Montemerlo M, Dahlkamp H, Stavens D, Aron A, Diebel J, Fong P, Gale J, Halpenny J, Hoffmann G, Lau K, Oakley C, Palatucci M, Pratt V, Stang P, Strohband S, Dupont C, Jendrossek LE, Koelen C, Markey C, Rummel C, van Niekerk J, Jensen E, Alessandrini P, Bradski G, Davies B, Ettinger S, Kaehler A, Nefian A, Mahoney P. Stanley: the robot that won the DARPA Grand Challenge. J Field Robot. 2006; 23(9):661–92.

23. Li X, Lehocky CA, Riviere CN. Efficient 3D control for needle steering using duty-cycled rotation. Proc 10th Int Conf Inform Control Autom Robot. 2013:192–9.

24. Christoforou, EG.; Seimenis, I.; Andreou, E.; Eracleous, E.; Tsekos, NV. Int J Med Robot. 2013. A novel, general-purpose, MR-compatible, manually actuated robotic manipulation system for minimally invasive interventions under direct MRI guidance. e–publication ahead of print

25. Reed KB, Okamura AM, Cowan NJ. Modeling and control of needles with torsional friction. IEEE Trans Biomed Eng. 2009; 56(12):2905–2916. [PubMed: 19695979]

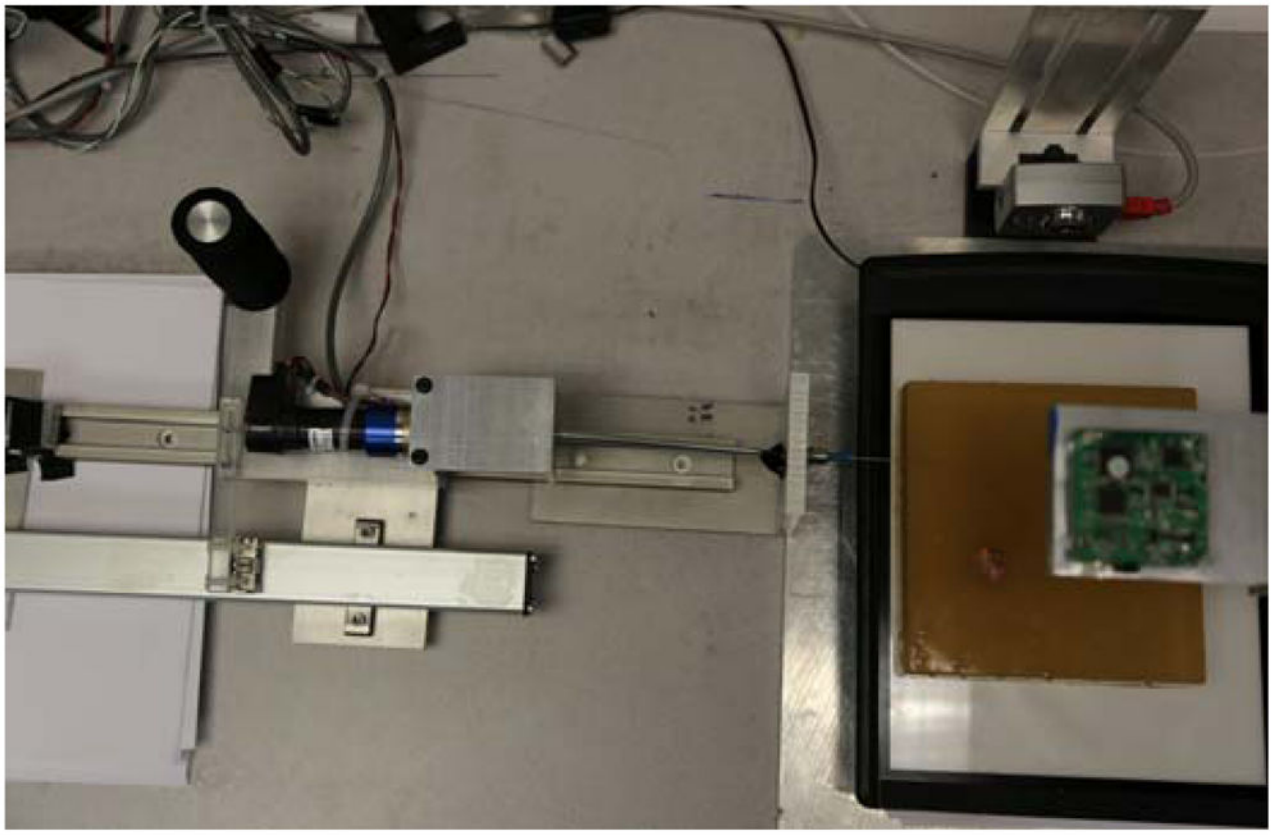

Figure 1.
Manual needle steering system. The user operates the handle on the left for insertion of the needle. A DC motor controls orientation and duty-cycled rotation of the needle. The needle is inserted into the tissue simulant, positioned in the view of orthogonal cameras.

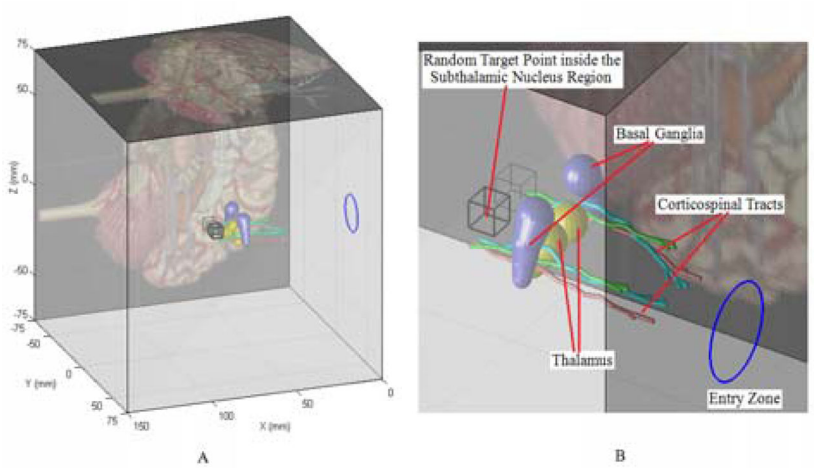

Figure 2.

The path planner pre-computes feasible paths in a human brain environment from entry zone to the target point located in the area of the subthalamic nucleus (indicated by a highlighted black bounding box), while avoiding anatomical obstacles along the paths. We try different target points (randomly generated) to test the planner. A: Overview of the environment. B: Close-up of the anatomical obstacles.

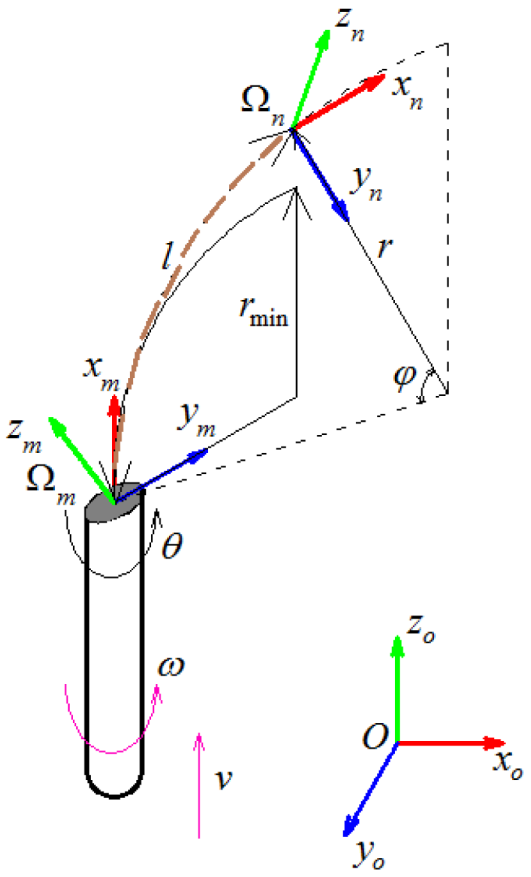

Figure 3.
Needle coordinate system, control inputs, and kinematics of curvature. The body coordinate frame is attached to the needle tip.

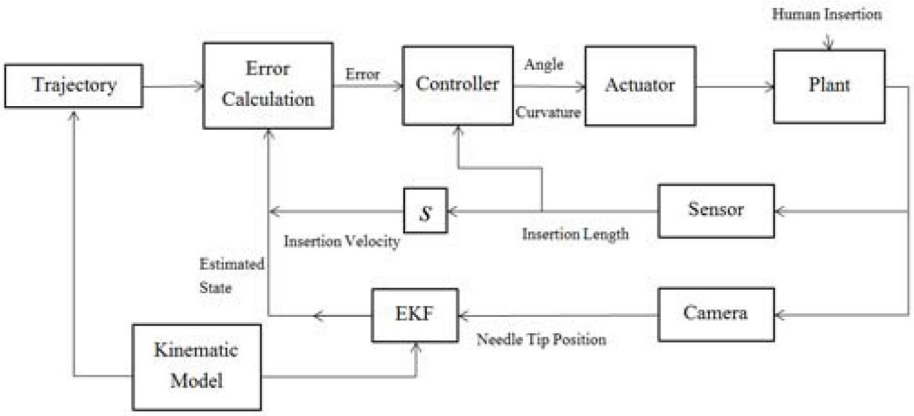

Figure 4.
Control block diagram for variable velocity needle insertion.

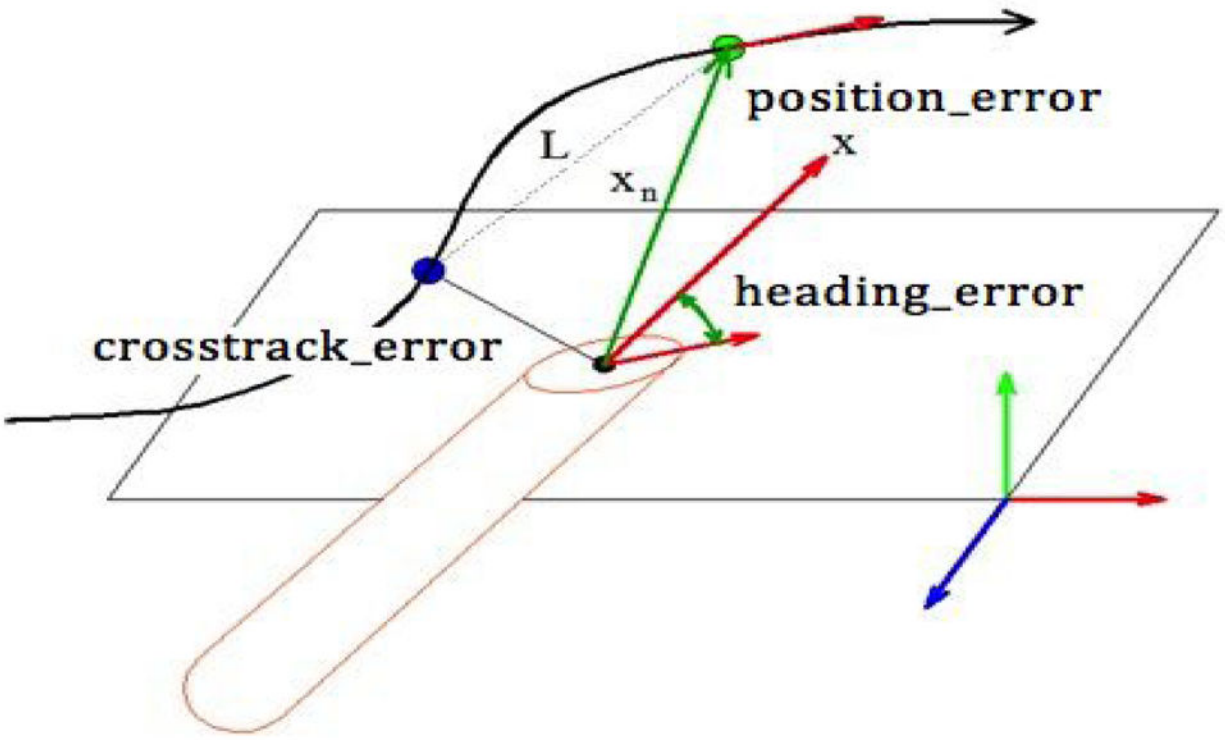

Figure 5.
Illustration of the two inputs for the proportional controller: modified crosstrack error [22] and heading error, as well as the position error for the look-ahead controller.

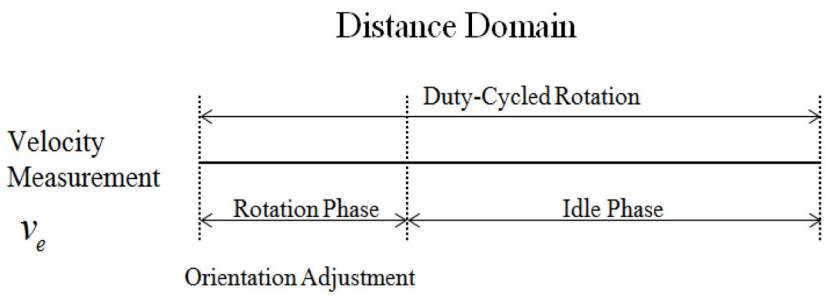

Figure 6.
One Cycle of Motor Control

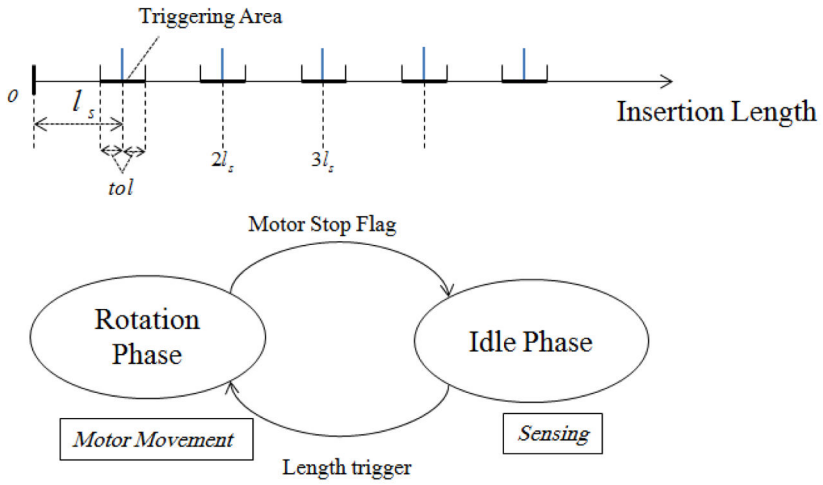

Figure 7.

Control state machine. As the needle is inserted, the scheme switches between a rotation phase in which the rotation motor is activated, and an idle phase consisting of pure insertion without rotation.

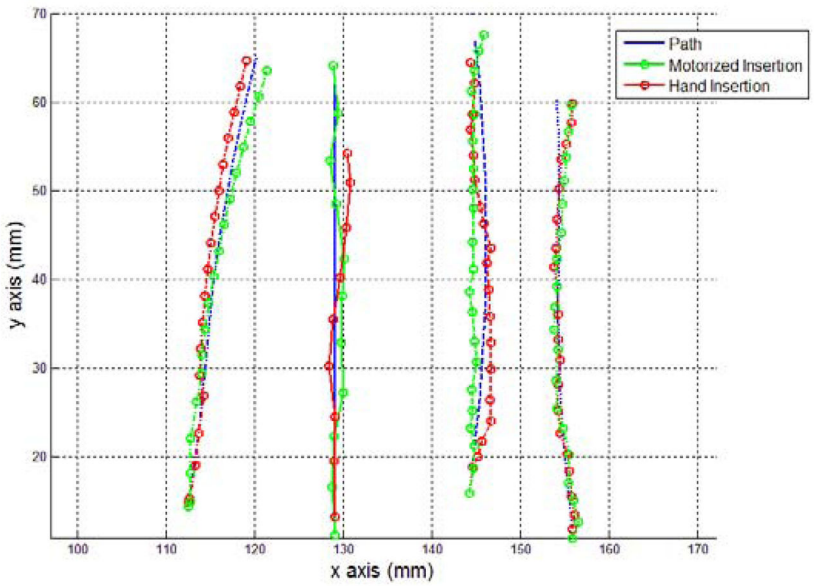

Figure 8.

2D results for different trials. Blue lines are preplanned paths, green lines with circle symbols are manual insertion results, and red lines with circle symbols are motorized insertion results.

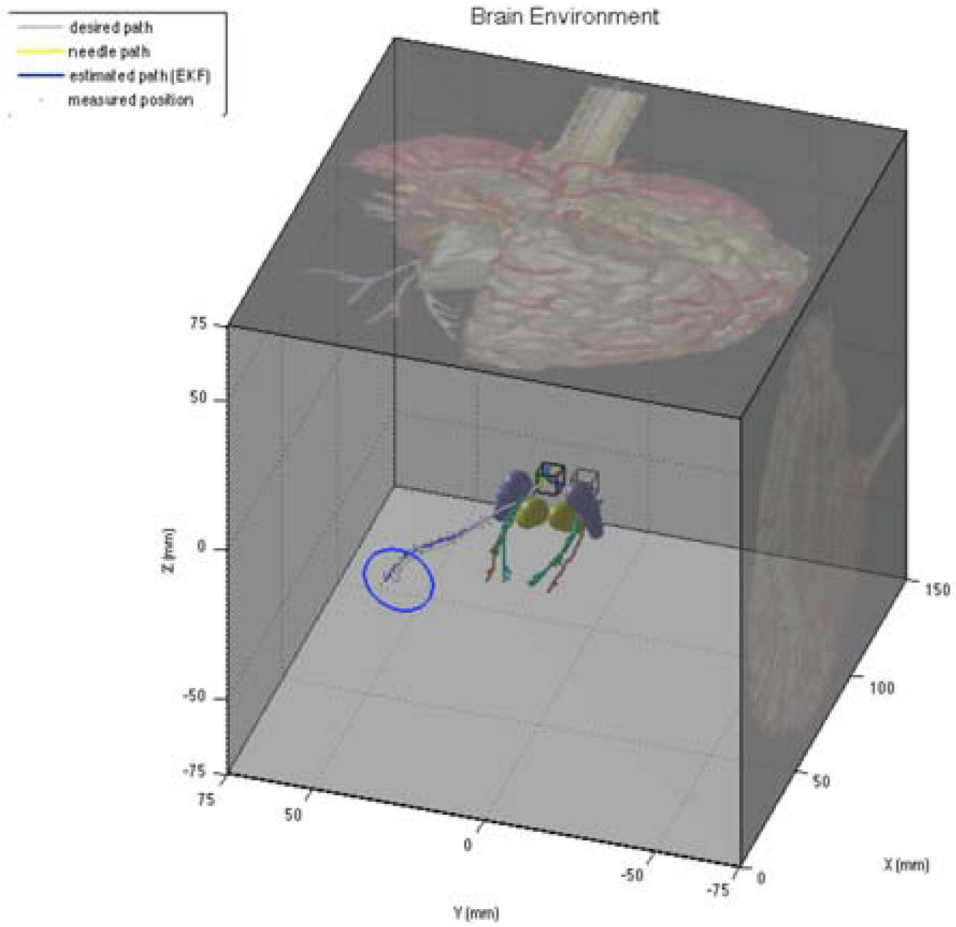

Figure 9.
Simulation of needle path following under variable insertion velocity control scheme.

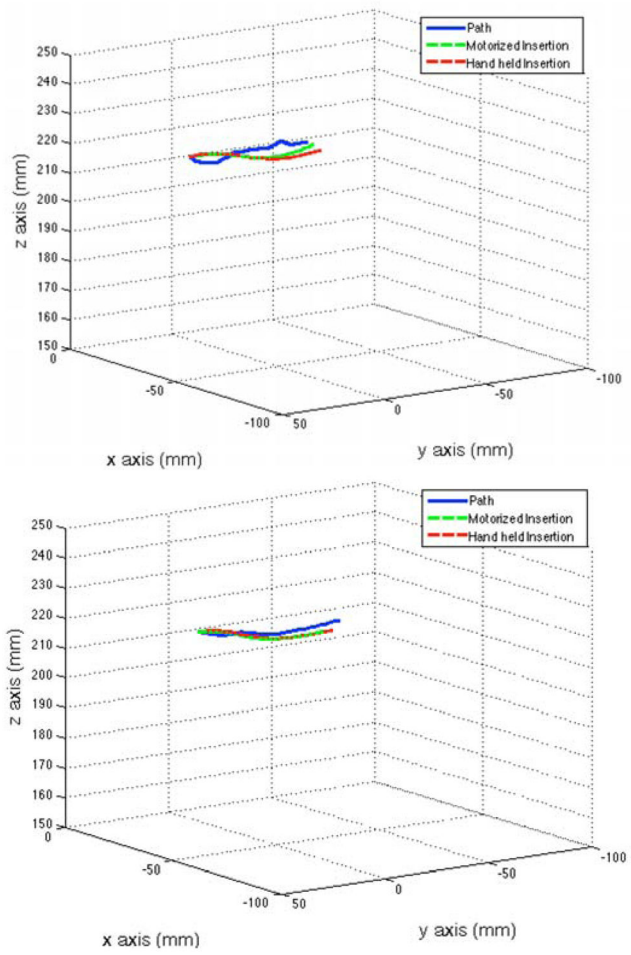

Figure 10.

Experimental results of 3D steering in tissue simulant. The two panels are results for two separate paths. The blue trace indicates the preplanned path, the red is the measured trajectory for manual insertion, and the green is the measured trajectory for motorized insertion.

TABLE I

Error of 2D Manual Insertion Experiments

Trial	Cross-track Error (mm)		Heading Error (rad)	
	RMS	*Maximum*	*RMS*	*Maximum*
1	0.86	1.31	0.07	0.17
2	1.87	2.74	0.08	0.19
3	0.22	0.79	0.04	0.11
4	1.30	1.12	0.06	0.04

TABLE II

Error of 3D Insertion Experiments

	Cross-track Error (mm)		
	RMS	***Max***	***Targeting***
Simulated	1.58	3.91	0.47
Motorized	3.41	4.97	3.37
Manual	4.59	7.50	7.22